Preprint
UCRL-JC-143473

Studies of Dynamic Failure of Steel Pipes Using X-Ray Radiography

M.B. Aufderheide, T.J. Orzechowski, J.D. Molitoris, A.J. Sunwoo, C.F. Cook, E. Urquidez, G.S. Dhillon, J.B. Chandler, M.R. de Haven, G.E. Steinhour, D.M. Slone, A.E. Schach von Wittenau, J.A. Jackson, H. Martz, D.M. Goodman

This article was submitted to the 28th Annual Review of Progress in Quantitative Nondestructive Evaluation (QNDE 2001) Brunswick, Maine, July 29 – August 3, 2001

U.S. Department of Energy
Lawrence Livermore National Laboratory

September 10, 2001

Review of Progress in Quantitative Nondestructive Evaluation, Vol. 21, 7/30 - 8/3 2001

STUDIES OF DYNAMIC FAILURE OF STEEL PIPES USING X-RAY RADIOGRAPHY

Maurice B. Aufderheide, Thaddeus J. Orzechowski, John D. Molitoris, Anne J. Sunwoo, Charles F. Cook III, Ernie Urquidez, Gurchan S. Dhillon, Jeffrey B. Chandler, Martin R. de Haven, Gary E. Steinhour, Dale M. Slone, Alexis E. Schach von Wittenau, Jessie A. Jackson, Harry Martz Jr., Dennis M. Goodman

Lawrence Livermore National Laboratory

Abstract. We describe an experiment which observed the failure of a steel pipe subjected to shock loading caused by the detonation of high explosive inside the pipe. The failure was observed using a variety of diagnostic probes, including optical and x-ray imaging. We describe and analyze the x-ray images in detail. Although the radiographs were damaged by fragment penetration, we see evidence that most of the fractures were due to shear failure rather than brittle failure. We also compare the static radiographs, taken just before the experiment, with simulations and do not yet see perfect agreement between them. The sources of this current lack of agreement are discussed, as well as the future work planned.

INTRODUCTION

The response of metals when they are subjected to shock loading is of great interest in a number of areas. In particular, the failure of metals under such extreme conditions is an area of active research[1,2,3]. Devising experiments that can probe this behavior is challenging because the phenomena happen quickly and typically produce a hostile environment (e.g. explosions). In such dynamic experiments, only the most robust diagnostic probes survive. In these experiments, the diagnostic goals are similar to those in nondestructive evaluation: we seek diagnostics that probe the object without perturbing it. Because these objects are typically breaking up, one might characterize the study of these objects as noninvasive evaluation, rather than nondestructive evaluation.

In this experiment, we subject a steel pipe filled with LX-10 high explosive to near-uniaxial hoop stresses (i.e. a radial stretch) by detonating the high explosive at one end. As the detonation front propagates up the high explosive, the metal cylinder is rapidly blown outward. The cylinder expands rapidly enough that the critical strain is reached and the pipe fractures. The characteristics of metal failure vary with the mechanism of failure and the type of alloy. In the case of shear failure, the stress becomes concentrated along grain or crystalline boundaries, resulting in the metal tearing along a direction roughly 45° to the surface. In brittle failure, the void concentrations in the metal coalesce, seeding a "v" shaped tear, which is perpendicular to the surface.

In these experiments, we seek to determine what kind of failure is occurring in the metal wall of the pipe as it is disassembling. Our main diagnostic for this effort will be radiography. In this paper, we describe the first experiment that produced useable radiographic images and discuss some analysis of the images. In the next section, we describe experimental setup and execution. In the third section, we describe some analysis of the radiographic images and, in the fourth section, we describe our efforts to simulate this system. In the last section, we conclude and describe future work.

EXPERIMENTAL SETUP AND EXECUTION

In this experiment, the 1045 steel pipe is 20 cm long, with a 5.08 cm outer diameter and a 3 mm thick wall. The cylinder has been annealed, oil quenched and tempered to provide a combination of strength and ductility[4]. A cylinder of LX-10 high explosive is press-fit into the pipe, with the detonator at the bottom of the cylinder. The detonation and disassembly are studied with a variety of diagnostics. Five Fabry-Perot interferometry beams measure the surface velocity of the expanding pipe. Two x-ray sources image the pipe at two different times. A soft capture apparatus stops a fraction of the fragments in a controlled manner to mitigate further damage in the deceleration process. The collected fragments are then available for further post-explosion metallographic analysis. In an earlier, identical experiment, a high-speed optical camera monitored the expansion, fracture and fragmentation of the metal cylinder in the visible wavelength regime. In this paper, we will show some optical images and discuss the x-ray images.

The experiment was performed in the 4" gas gun tank at LLNL's High Explosives Applications Facility (HEAF). The gun tank provided protection against the shrapnel produced by the experiment. A steel cylindrical fragment catcher two inches thick with a three-foot outer diameter provided additional protection. Holes were cut out of the fragment catcher for the x-ray windows. These apertures used lexan and aluminum plates to stop the fragments.

The x-ray sources were Scandiflash 450 keV bremsstrahlung sources. These sources produce doses of approximately 30 mRoentgen at one meter and have a spot size full-width at half maximum of approximately 1 mm. These sources were chosen because of their relatively large dose and energetic spectrum. Both properties were needed to penetrate the steel pipe and the fragment protection.

The detection medium for this experiment was a film pack, containing three sheets of Biomax film. The top and bottom sheets each were inserted between Kodak Lanex screens that faced inward toward the film. The middle sheet of film faced away from the Lane screens. After exposure, the films were developed using an automated processing machine and then digitized using a Perkin-Elmer 1010GM microdensitometer with square 200 μm pixel size. Fog levels for the film were estimated by processing an unexposed piece of film.

We used two x-ray sources that were approximately 203 cm (80 inches) from the center of the pipe and in the same plane as the middle height of the pipe. The sources were about 91 cm (36 in) apart and pointed at the axis of the pipe. The film pack was located 61 cm (24 in) behind the pipe. The film was a rectangular sheet 71 x 28 cm^2 (28 x 11 in^2) in size. The source and film locations were selected so that the image from each source did not overlap with the other. A 5 cm (2 in) thick steel collimator was placed between the source and pipe in order to limit illumination of each view by its neighbor. The x-ray sources were timed so that images were captured after 16.5 μs and 26.4 μs of evolution time.

The steel fragment catcher, except where the x-ray windows were cut, provided shrapnel protection. The film was protected by ¾" of aluminum plate and ½" lexan, placed in front of the pack. The sources were shielded by ½" of aluminum plate and 1/8" of lexan.

Optical images of an identical exploding pipe were obtained using a Cordin camera in an earlier experiment. This camera took approximately sixty images at a rate of one

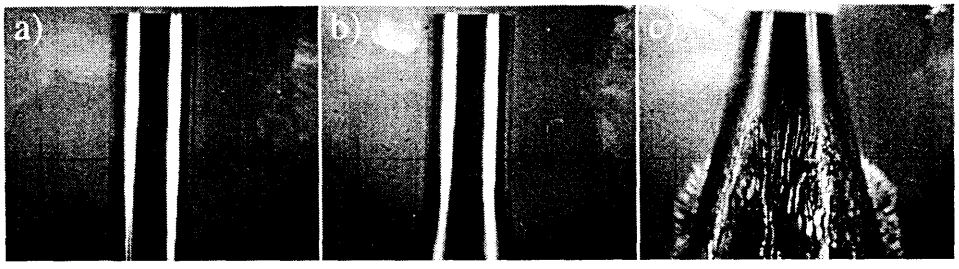

Figure 1 Optical images of the cylinder expansion. Initial image (a), image at 16.5 μs (b), and image at 26.4 μs (c). Times b) and c) correspond to the times at which the radiographs were taken. Note the break-up is definitely visible in (c).

frame/μs. Mirrors were used to relay the image of the pipe to the camera, which was outside the chamber. This optical image was parallel to the radiographic view.

The steel cylinder had been heat-treated to make the steel harder and it was polished to a 32 μinch finish. Optical images are displayed Figure 1. The shine of the pipe before high explosive detonation in Figure 1a) attests to the finish. Figure 1b) shows the pipe when the detonation front is roughly 1/3 of the way up the pipe at which time the first radiograph was taken. Figure 1c) shows the pipe when the detonation front is roughly is roughly 2/3 of the way up the pipe, at which time the second radiograph was taken. Cracks are definitely visible in the third image, while there are hints of cracks in the second image. A bright flash is visible at the top of the cylinder in Figure 1c), which is light from the reaction front shining out of the top of the cylinder.

The fragments from the exploding pipe were extremely energetic and made ¼" deep gouges in the steel fragment catcher. Based on analytic estimates using the Gurney velocity[5] and 2D arbitrary Lagrangian-Eulerian[6] hydrodynamic simulations, the fragments had a velocity of about two mm/μs. The fragments were so energetic that they penetrated the fragment protection and damaged the film packs. The resulting images are displayed in Figure 2. The dynamic images have been thresholded so that the cracks can be seen in both images. It can be seen from Figure 2b) that the earlier dynamic image was most badly damaged by fragments. Only a small portion of the image near the bottom has been uncompromised. Figure 2c) has been less badly damaged. Much of the cracked region is still visible, as well as some of the region near the detonation front.

RADIOGRAPHIC ANALYSIS

The images shown in Figure 2 are the result of the microdensitometer scans. As noted above, unexposed film was also scanned. It was found that the fog level of the film was 0.245 optical density units. The static image (Figure 2a)) had film densities ranging from 0.8 to 2.9. The unobscured regions of the image had densities ranging from 2.5 to 2.9. The center of the pipe had densities on the order of 1.0, so that our signal is well above the film fog background. Similar film densities were measured in the parts of the two dynamic images which are farthest from the fragment damage.

There is evidence that the film was darkened as a result of the fragment penetration, as well as from the x-rays. This darkening occurred over a much broader region than just the immediate vicinity of the penetrations. Evidence for this effect can be seen in lineouts of the Figure 2c) along the symmetry axis of the cylinder. Near the bottom and

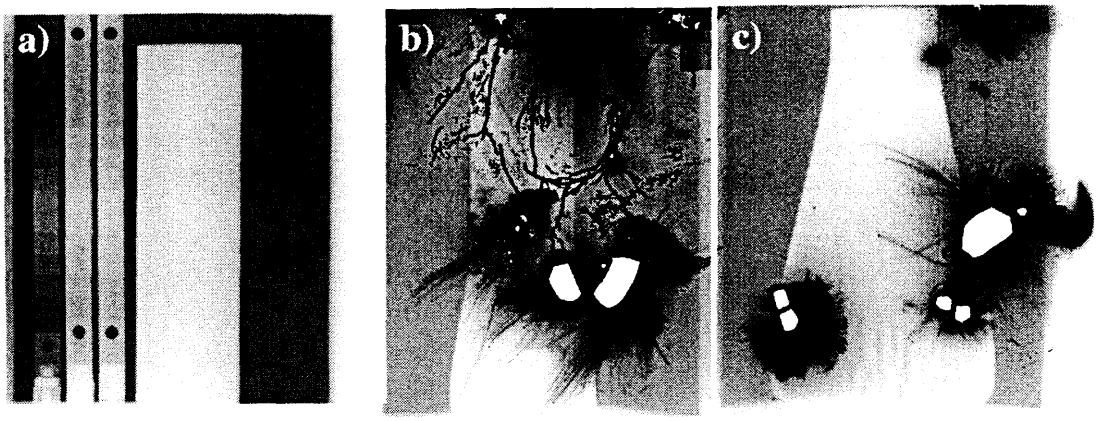

Figure 2 Radiographs of the pipe before the detonation (a), 16.5 μs after the detonation (b), and 26.4 μs after detonation (c). Step wedges were included in the static radiograph (a), but removed before detonation. The white regions in (b) and (c) are where the film was punctured by the fragments. Damage to the film can be seen to extend far beyond the actual penetration points.

top of the radiograph the film density has a value of approximately 1. The constancy of this value is not surprising, because the x-rays still have to pass through the same amount of cylinder material, even if it is expanded. Between the two clusters of fragment penetrations, however, the film density increases to 1.5. The film has been darkened either because of a pressure pulse hitting the film, or because the Lanex screens have produced extra light in response to the pressure pulse. This effect limits our ability to quantify the depth of the cracks in the image. However, we can still count the cracks that are visible and examine their properties. We also can analyze the static image, in order to see how well we can quantify future radiographs in which the fragments do not hit the film.

We begin by analyzing the current dynamic radiographs. It can be seen in the dynamic images that the cylinder expands outward such that the deformed pipe is a cone with a definite opening angle. This opening angle, known as the Taylor angle, is interesting to measure because it is a sensitive function of the detonation front velocity and the densities of the steel and high explosive. We determine this angle in Figures 2b) and 2c) by measuring the location of the left edge of the pipe in each radiograph at two points which were not obscured by fragment damage.

We have found that the true edge of the pipe in the radiograph is most accurately determined by finding the point at which the gradient of the radiograph is changing the most rapidly. This approach was verified empirically by observing the static portion of the pipe, for which we know the width. The edge of the pipe is not the point at which the radiograph begins to show a reduction of x-ray flux, because the finite size of the source, as well as finite film resolution, causes some blurring of edges in the radiograph. The accuracy of edge determination is roughly 1%. Using these techniques, we determine a Taylor angle of 10° for the first, earlier, image and 13° for the second image. These results are in excellent agreement with the hydrodynamic simulations mentioned above, but do not agree with an analytic estimate.

It is also useful to determine the velocity of the cylinder, after being accelerated by the high explosive detonation. We do this by comparing the location of the lower left edge of the pipe, relative to its axis of symmetry, in the two radiographs. The radiographs are 9.9 μs apart, so that the ratio of the edge displacement to the time difference is an estimate of velocity. This estimate is accurate because, after the high explosive impulse, the cylinder

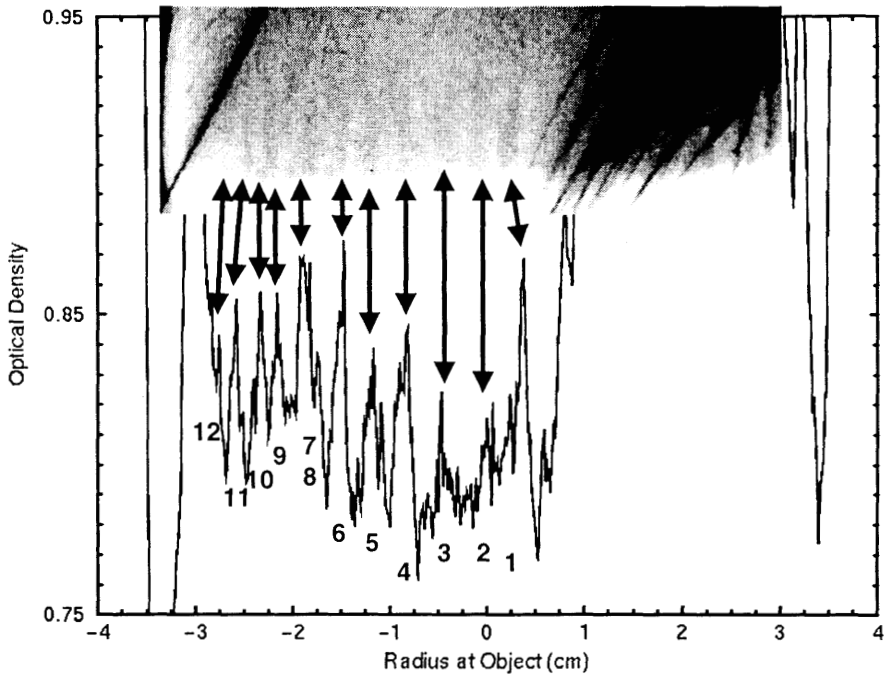

Figure 3 Close-up of first dynamic image and plot of the average of ten image rows across the image. The left edge of the pipe is seen at far left. The black regions are damage from fragments. Note the sharpening of the peaks as the view into the pipe becomes more oblique.

travels ballistically, experiencing no further accelerations. We measure a displacement of 1.8 cm, indicating a wall velocity of 1.9 mm/μs. The uncertainty in this measurement is roughly 10%, with half the uncertainty coming from the displacement determination and half from the timing. This estimate is in excellent agreement with the prediction from the hydrodynamic simulation. It also agrees with the analytic estimate using the Gurney velocity.

A measure of the expansion of the cylinder is given by the strain, which is the ratio of the change in radius of the cylinder to the original cylinder radius. In Figure 2b), the largest strain occurs near the bottom of the image, and has a value of 0.41+/- 6%. In Figure 2c), the largest strain is 1.13 +/- 4%, again seen near the bottom of the image.

Both radiographs show evidence of the failure of the pipe in the form of a series alternating dark and light stripes roughly parallel to the pipe symmetry axis in the region of maximum strain for each image. There are no similar features in the static radiograph. The very dark region on the right side of the image is the start of bad damage from fragment penetration. In Figure 3, we display a portion of the early time dynamic radiograph centered on the region of maximum strain. The left edge of the pipe is visible on the far-left side of the image. The dark band near the left edge of the image another artifact of fragment damage. The vertically oriented striations are clearer. In addition, we display an average of 10 contiguous rows near the center of this image. In this plot, the optical density in the image is plotted versus the radial location in the plane of the pipe. In this horizontal lineout, the cracks are clearly visible as regions of greater optical density. Twelve distinct cracks are labeled across the lineout. The two peaks just to the right of crack number one are artifacts from fragment damage and are not counted as cracks.

A striking feature of the image is that the sharpest cracks are near the limb (radius far from zero) of the cylinder, rather than near the center (radius near zero). This is somewhat surprising, because, with radiography, features in a pipe are usually best seen

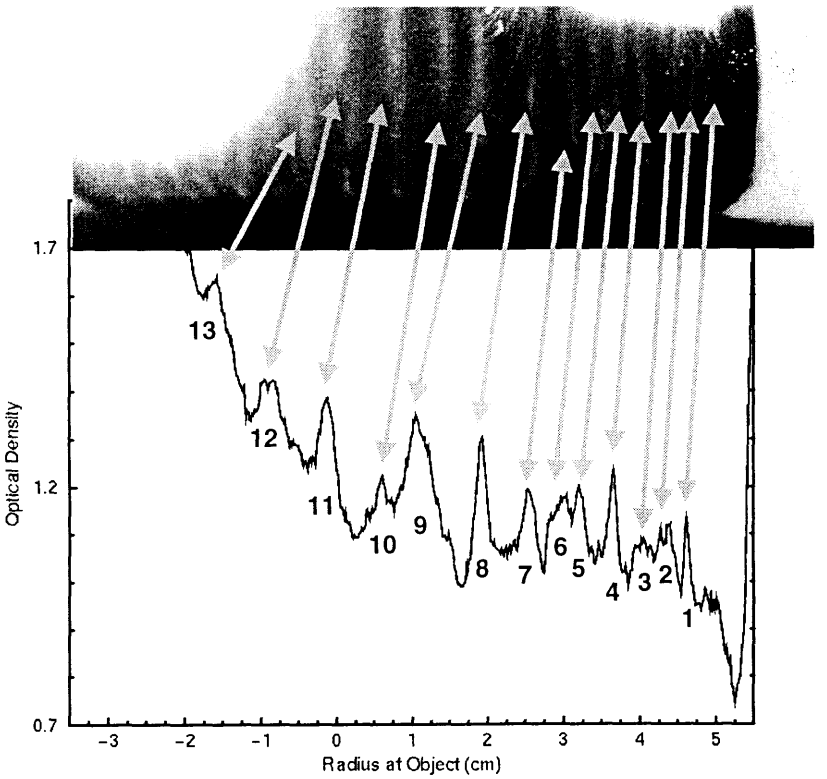

Figure 4 Close-up of second dynamic image and plot of the average of ten image rows across the image. The right edge of the pipe is seen at far right. The black regions are damage from fragments. Note the sharpening of the peaks as the view into the pipe becomes more oblique.

when the view is nearest the central radius of the pipe. As the view becomes more oblique (i.e. near the limb), there is greater blurring out and confusion of features. Such features would be more visible on the limb if the cracks in the pipe were not strictly radial through the pipe, but were at an oblique angle, such as 45°, to the radial direction. In such a case, the cracks near the central radius would be visible, but less distinct, because the x-rays would not be directly aligned with the crack. As the view of the pipe approached 45°, either the cracks would become maximally sharp, or maximally indistinct, depending on which direction to the radial the oblique cracks appeared. Figure 3 shows that our experiment was lucky in that the oblique cracks pointed toward the x-ray source. It is also apparent that the cracks nearer the limb are closer together, confirming the sloping of the pipe away from this field of view. The oblique orientation of the cracks is significant because it indicates that most of the failure in the pipe was due to shear failure, rather than brittle failure.

In Figure 4, we look in detail at the later dynamic image, near the region of maximal strain. In this image, we see more of the right side of the cylinder. The right edge of the pipe can be seen on the far right of the image. Fragment damage blots out the those in Figure 3, although the sharpening of the cracks at oblique views is not as striking. It may be that the cracks are pointed away from this field of view. In this image, we see thirteen cracks.

Both radiographs are seeing the front and back pipe surfaces, projected onto a single image. Thus it is not possible to determine which cracks correspond to which surface. Here we assume that each surface contributes half of the cracks. By calculating what fraction of the total pipe circumference we are seeing in each image, and extrapolating

this back to the original pipe radius, we are able to estimate a crack frequency for each image. From Figure 3, we estimate that a crack occurred every 0.5 cm around the original pipe. From Figure 4, we estimate that a crack occurred every 0.6 cm around the original pipe. The uncertainty in these estimates is large enough that the values are consistent. We estimate an uncertainty in the number of counted cracks to be one to two cracks, because it is occasionally not clear whether two close cracks, or one single large crack, are being observed. Another source of uncertainty is whether we are completely missing crack oriented in the maximally indistinct orientation.

We included a series of step wedges in the static image, Figure 2a). The rightmost wedge was a steel wedge, the leftmost wedge was lexan, and the middle wedge was steel in front and lexan in back. Steel was used to study the attenuation properties of the steel pipe. Lexan was a surrogate for the high explosive. The two materials were combined in the middle wedge in order to see how the combination of materials affected attenuation. The thicknesses of the step wedges are listed in Table 1. Each wedge was designed in a "ziggurat" style, with the thickest step near the center of the wedge and thinner steps alternating above and below this step. Starting from the top of the image, the order of the steps is 1, 4, 6, 8, 10, 9, 7, 5, 3, and 2.

Table 1 Thickness of step wedges, in cm.

	Steel	Lucite
1	0.6365	0.635
2	0.6381	0.635
3	0.7568	1.27
4	0.8757	1.905
5	0.9927	2.54
6	1.1151	3.175
7	1.2316	3.81
8	1.3518	4.445
9	1.469	5.08
10	1.5882	5.715

We have analyzed the static image in more detail, because it was not compromised by fragment damage. The static image was taken using a single flash from each x-ray head. In Figure 2a), the neighboring source produced an image further to the left on the film. The steel collimator strongly reduced the contribution of the neighboring source to the field of view shown in Figure 2a). However, scattering from this neighboring radiographic view was seen on the left side of the image. This contribution was fit and subtracted from the image, after the fog level also was subtracted. Next, the beam profile was fit using roughly 40 points in the image, which were unobscured by the wedges or cylinder. This beam fit was then divided out of the image, resulting in an I/I_0 image. Figure 2a) is the result of this postprocessing.

After all of these manipulations, the cylinder image was examined along its symmetry axis. If all flat-fielding operations were successful, the I/I_0 values should be constant along lineouts that are parallel to the symmetry axis. This was not found to be the case. Instead, the transmission through the pipe ranged from 20% near the bottom of the pipe to 35% near the top of the pipe. This variation in transmission indicates that there is roughly a 10% component to the x-ray beam that does not correspond to direct radiation. It is likely that Compton scattering somewhere in the system is causing this additional signal. We do not believe that this signal is direct radiation from the neighboring source, because its effect appears to die off near the center of the step wedges. There are many steel and aluminum plates in the system and it is likely that both sources are producing a great deal of Compton glow as their radiation passes through these plates. This artifact has made quantitative comparison with simulation very difficult.

SIMULATION EFFORTS

Radiographic simulation is useful because it allows the user to study isolated aspects of the problem and to optimize future experiments. In addition, simulation would allow

us to determine how the orientation of cracks relative to the x-ray beam affects their visibility. We are hoping to use these experiments to help validate the accuracy of our simulations. In this work, we have been using the HADES radiographic simulation code[7]. HADES is a ray-tracing code that can use detailed models for source spectra and detector response to model the radiographic imaging process quantitatively.

We have used the MCNP4B Monte Carlo code[8] to model the source and the detector. The source was modeled by sending a zero-width beam of 450 keV electrons into the tip of a tungsten cone. The spectrum (with 43 energy bins) was collected using a point detector 1 m downstream. $7x10^6$ electrons were run so that the variance within each bin was well below 1%. HADES uses this spectrum for its calculation of pathlength as a function of source energy.

The detector was modeled as a film/Lanex screen combination. The second Lanex screen has not yet been included in the simulation. Fifteen energy bins up to 450 keV were used for modeling this detector. In modeling this detector, the energy deposit in the Lanex was computed. It was then assumed that this energy deposit was directly proportional to the film density captured on the film. Our modeling of detectors has been reported in more detail elsewhere[9].

Using these models, HADES predicts a transmission of 6% through the steel pipe, while experimentally we see 20%. This disagreement is disappointing, but there are still a number of possible explanations. It could be that there is more scattering in the image than expected. In this case, the 20% to 35% variation in transmission would be a scattering effect sitting on top of the direct signal. Another explanation could be that the spectrum is too soft because we have missed some metal shielding in the field of view. If there were additional shielding in the system not included in the simulation, the experiments would show more spectral hardening than the simulation. We have included all of the shielding discussed above. Another possible explanation is that the source simulation does not accurately represent the tungsten tip used in the Scandiflash machines, resulting in a spectrum that is too soft. Another possibility is that we need to include both Lanex screens in the simulation of detector properties. A last possibility is that our assumption of direct proportionality between the energy deposit in the Lanex screen and film density is incorrect. We hope that the three different step wedges and the pipe will allow us to determine which of these possibilities is the case.

CONCLUSIONS AND FUTURE WORK

In this experiment, we have seen that radiography is a potentially useful probe of metal failure under extreme conditions. The current experiment has probed some details of metal failure, but the approach is new and needs refinements. First, we need to ensure that fragments do not hit the detector in future shots. Second, we need to continue our analysis of the static radiographs, in order to determine how well we understand the attenuation seen in the image. Even with these uncertainties, we see strong evidence in the radiographs that shear, rather than brittle, failure is occuring in these pipes. This is a very significant finding.

In order to refine these techniques, future radiographic shots are planned. Some of these shots will be done with x-rays, while some will be done with 800 MeV protons. The use of different radiographic probes will provide more insights into what we are seeing.

Radiographic analysis will continue. The wealth of step wedge data from the static image hopefully will allow us to determine why our current simulations are overpredicting attenuation. We will refine our detector model and seek out any missed shielding. We will also seek to model the source more accurately. In addition, we will continue analysis of the dynamic images, in order to extract more information about the failure of the pipe.

ACKNOWLEDGMENTS

MBA thanks Peter D. Barnes Jr., for the use of his step wedges. Some of this work has been funded in part by a Laboratory Directed Research and Development exploratory research grant provided by the Engineering and Defense and Nuclear Technologies Directorates. This work was performed under the auspices of the U.S Department of Energy by the University of California, Lawrence Livermore National Laboratory under Contract No. W-7405-Eng-48.

REFERENCES

[1] Grady, D. E., *Mechanics of Materials*, **29**, 181-203 (1998).
[2] Davidson, L., Grady, D. E., and Shahinpoor, M., eds., *High-Pressure Shock Compression of Solids II: Dynamic Fracture and Fragmentation*, Springer, 1995, articles within.
[3] Zurek, A. K., and Follansbee, P. S., *Metallurgical and Materials Transactions*, **26A**, 1483-1490 (1995).
[4] Rosen, R. S., Kassner, M. E., Thiehsen, K. E., *Journal of Material Science Letters*, **11**, 125-128 (1992).
[5] Gurney, R.W., *The Initial Velocities of Fragments from Bombs, Shells, and Grenades*, Ballistic Research Laboratory, Aberdeen, Maryland, BRL-405, 1943.
[6] Barton, R. T., in Numerical Astrophysics, edited by J. M. Centrella, J. M. Le Blanc, and R. L. Bowers, Jones and Bartlett Publishers Inc., Boston 1985, 482ff.
[7] Aufderheide, M. B., Slone, D. M. and Schach von Wittenau, A. E., "HADES, a radiographic simulation code", in *Review of Progress in Quantitative Nondestructive Evaluation*, edited by D. O. Thompson and D. E. Chimenti, AIP Conf. Proc. #557, Vol. 20A (2000), pp. 507-513.
[8] Briesmeister, J. F., "MCNP^{TM}--- a general Monte Carlo n-particle transport code", Technical Report LA-13709-M, Los Alamos National Laboratory (2000).
[9] Schach von Wittenau, A. E., Logan, C. M., Aufderheide, M. B. and Slone, D. M., Med. Phys., submitted.